



Published in final edited form as:

Nat Methods. 2014 April ; 11(4): 456–462. doi:10.1038/nmeth.2854.

Gold rotor bead tracking (AuRBT) for high-speed measurements of DNA twist, torque, and extension

Paul Lebel^{1,2}, Aakash Basu^{1,2,5}, Florian C. Oberstrass², Elsa M. Tretter^{3,6}, and Zev Bryant^{2,4}

¹ Department of Applied Physics, Stanford University, Stanford, California, USA

² Department of Bioengineering, Stanford University, Stanford, California, USA

³ Department of Molecular and Cell Biology, University of California, Berkeley, California, USA

⁴ Department of Structural Biology, Stanford University Medical Center, Stanford, California, USA

Abstract

Simultaneous measurements of DNA twist and extension have been used to measure physical properties of the double helix and to characterize structural dynamics and mechanochemistry in nucleoprotein complexes. However, the spatiotemporal resolution of twist measurements has been limited by the use of angular probes with large rotational drags, preventing the detection of short-lived intermediates or small angular steps. Here we introduce AuRBT, demonstrating a >100X improvement in time resolution over previous techniques. AuRBT employs gold nanoparticles as bright low-drag rotational and extensional probes, relying on instrumentation that combines magnetic tweezers with objective-side evanescent darkfield microscopy. In an initial application to molecular motor mechanism, we have examined the high-speed structural dynamics of DNA gyrase, revealing an unanticipated transient intermediate. AuRBT also enables direct measurements of DNA torque with >50X shorter integration times than previous techniques; here we demonstrate high-resolution torque spectroscopy by mapping the conformational landscape of a Z-forming DNA sequence.

Users may view, print, copy, and download text and data-mine the content in such documents, for the purposes of academic research, subject always to the full Conditions of use:http://www.nature.com/authors/editorial_policies/license.html#terms

Correspondence should be addressed to Z.B. (zevry@stanford.edu).

⁵Present Address: Howard Hughes Medical Institute and Laboratory of Sensory Neuroscience, The Rockefeller University, New York, New York, USA

⁶Present Address: Nurix Inc., San Francisco, California, USA

Author contributions

P.L. designed and built instrumentation, wrote data acquisition code, performed experiments, and analyzed data. A.B. aided in developing and interpreting DNA gyrase experiments, collaborated on data acquisition code, and performed calibration experiments to establish evanescent nanometry procedures. F.C.O. synthesized molecules for torque spectroscopy and aided in static torque assay development. E.M.T. purified and characterized *E. coli* GyrA and GyrB subunits for gyrase experiments. Z.B. conceived and supervised the project. P.L. and Z.B. wrote the paper. All authors discussed the results and commented on the manuscript.

COMPETING FINANCIAL INTERESTS

The authors declare they have no competing financial interests.

Introduction

Single molecule tracking experiments can yield rich information about the structural dynamics of a molecular system, but are fundamentally limited by Brownian noise^{1,2}, which must be overcome in order to resolve discrete transitions on biologically relevant timescales. To analyze structural transitions in DNA:protein complexes, several groups have introduced real-time methods for simultaneously measuring two broadly relevant structural properties³: changes in DNA contraction (Δz) caused by bending⁴, stretching, or sequestering DNA contour length; and changes in linking number (ΔLk) due to trapped writhe (as in gyrase⁵⁻⁷ or nucleosome^{8,9} wrapping), trapped twist deformations (such as DNA unwinding within transcriptional complexes¹⁰ or recombination filaments¹¹⁻¹³), or topoisomerization¹⁴. Direct measurements of ΔLk rely on observing the rotation of a probe attached to the DNA molecule^{12,13,15}; the spatiotemporal resolution of these measurements depends on the rotational hydrodynamic drag of the probe³. To date, the highest resolution angular measurements have been achieved using rotor bead tracking (RBT)^{3,6}, which takes advantage of probe specialization: a micron-scale magnetic bead is used to apply pN-scale forces to stretch the DNA, while a lower-drag secondary probe bound to the side of the molecule (the “rotor bead”, typically a ~300 nm polystyrene sphere) reads out molecular twist and extension. RBT achieves subsecond relaxation times. However, angular steps smaller than half a rotation ($\Delta Lk = 0.5$) have required several seconds to distinguish from noise⁶. Currently, RBT and alternative methods such as Freely Orbiting Magnetic Tweezers (FOMT)¹³ are thus inadequate for observing unitary steps and substeps in the unperturbed milliseconds-to-seconds timescales typical of many biological processes^{6,16,17}.

Torque resolution suffers from a closely related limitation^{3,18}. Direct torque measurements¹⁹ have been used to quantify the torsional rigidity of DNA²⁰⁻²², study the plectonemic buckling transition²¹⁻²⁵, and analyze sequence-dependent structural transitions^{23,26}. However, current methods require at minimum seconds of integration — typically much longer than this — to achieve biologically relevant torque precisions on the order of 1 pN nm^{3,18,23,26}. In the Brownian-limited regime, drag is the only parameter influencing torque noise density³. Torque measurement methods that use low-drag probes are thus needed for high-resolution torque spectroscopy and for studies of torque generation by molecular motors that unwind²⁷, supercoil⁵, or helically track¹⁵ DNA.

Here, we have further exploited probe specialization to achieve large gains in spatiotemporal resolution over RBT. Using 80-140 nm gold particles as rotors, AuRBT reduces rotational drag by orders of magnitude over existing methods^{3,6,13,21-23,26,28}, enabling torque and twist measurements on the millisecond timescale and reduced Brownian noise over longer timescales. AuRBT includes a simultaneous readout of molecular extension using evanescent nanometry^{29,30}, providing a second degree of freedom with which to monitor nucleoprotein dynamics. We illustrate AuRBT's enhanced spatiotemporal resolution with three application experiments. First, we demonstrate the detection of subtle helicity changes induced by changes in DNA tension, due to twist-stretch coupling. Next, we present a high-resolution study of DNA gyrase, revealing a previously unknown structural substate. Finally, we use AuRBT torque spectroscopy to map the B-Z transition in a short DNA sequence, and show that the increased torque resolution provides the sampling power to

measure torque probability distributions for meaningful comparisons to theoretical predictions.

Combined evanescent scattering and magnetic tweezers

AuRBT uses darkfield microscopy to track the 3D position of a gold nanoparticle that is bound to the side of a stretched DNA molecule (**Fig.1a-c, Supplementary Video 1**). Gold nanoparticle tracking has previously been implemented using a variety of darkfield configurations, including designs relying on laser illumination through a condenser^{31,32} and both prism-type³³ and objective-type³⁴⁻³⁷ evanescent excitation. Here we have chosen evanescent excitation so that a nanoparticle can be imaged adjacent to the surface without contamination from scattering by the larger magnetic bead attached to the opposite end of the DNA molecule. We chose objective-side illumination in order to accommodate magnetic tweezers on the condenser side of the sample. In a departure from previous work³⁴⁻³⁶, our implementation uses two small 45° mirrors positioned below the objective to couple laser excitation both in and out of the sample at high numerical aperture³⁷ (**Supplementary Figs. 1,2**), similar to a design previously used for multi-wavelength fluorescence measurements³⁸. The scattering image is collected on an EMCCD camera at high frame rates (up to 6.3 kHz); the instantaneous angle can then be determined from in-plane coordinates of the rotor (**Fig. 1b**), and vertical displacements of the rotor can be calculated using evanescent nanometry^{29,30} (**Supplementary Fig. 3**).

Small probes reduce integration time by orders of magnitude

AuRBT detects small twist signals by rapidly averaging over Brownian noise. Using rotor beads with radii several times smaller than previous methods has reduced drag by nearly two orders of magnitude, achieving angular diffusion constants in excess of 1,000 rad²/s. The highest resolution measurements shown here use 80 nm rotor beads and 420 bp DNA tethers (“AuRBT-80nm/420bp”), exhibiting a ~1 ms relaxation time and enabling precise twist determination >200X faster than currently published techniques^{3,6}.

For Brownian-limited DNA twist measurements, the signal-to-noise ratio (SNR) depends on the extent to which fluctuations can be reduced from their full-bandwidth amplitude of $(k_B T / \kappa)^{1/2}$ given by equipartition. Analogous considerations have been extensively reviewed for the case of extension measurements^{1,2}. Angle measurements are correlated over the relaxation time $t_r = \gamma / \kappa$, where γ is the drag of the probe and κ is the torsional stiffness of the tether. Fast relaxation times permit rapid sampling of fluctuations; therefore, in any given time interval, higher SNR can be achieved by either reducing drag or stiffening the tether. The expected RMS noise σ for a signal integrated over time t is given by the expression below, plotted as solid lines in **Figure 2a**^{39,40}:

$$\sigma = \sqrt{\frac{2k_B T}{\kappa} \left(\frac{t_r}{t} - \left[\frac{t_r}{t} \right]^2 \left(1 - \exp\left(-\frac{t}{t_r}\right) \right) \right)} \quad (1)$$

Measurements of RMS noise as a function of integration time confirm the expected performance of AuRBT (**Fig. 2**). The relaxation time t_r for AuRBT ranges from ~1-10 ms

depending on the bead and tether chosen (**Supplementary Table 1**). The large- t limit ($t \gg t_r$) illustrates how spatiotemporal resolution is affected by drag:

$$\sigma \approx \sqrt{\frac{2k_B T \gamma}{\kappa^2 t}} \Rightarrow t \approx \frac{2k_B T \gamma}{\kappa^2 \sigma^2} \quad (2)$$

In order to detect a given step size with a given signal-to-noise ratio, the required integration time thus scales linearly with drag, which in turn depends on the cube of the probe diameter. AuRBT provides biologically relevant gains in resolution. For example, previously published techniques would require >20 s of integration to detect the angular signal corresponding to unwinding of a single basepair ($|\Delta Lk| = 0.095$), such as could result from unitary steps of RNA polymerase^{10,15,16}. Using AuRBT, this measurement can be performed in ~80 ms with SNR = 3 (**Fig. 2a**). (Several studies have discussed the SNR needed for step detection and measurement in single molecule experiments, and have recommended minimal values ranging from SNR = 2 to SNR = 6 for various stepfinding algorithms and detection criteria^{1,41-44}.) For an alternative representation of resolution comparisons, noise power spectral density plots are shown in **Supplementary Figure 4**.

Cubic scaling of drag with particle size was confirmed by plotting all measured angular diffusion constants as a function of measured bead diameters (**Fig. 2c**). A global fit to the approximate expected relationship $D = k_B T / (14 \pi \eta r^3)$ gives an effective viscosity $\eta_{eff} = 1.2$ mPa s — slightly higher than the viscosity of the bulk solution, as may be expected due to the proximity of the surface (see **Supplementary Fig. 5**).

Rapid measurement of twist-stretch coupling in DNA

We challenged the high twist resolution of AuRBT by measuring a known physical property of the double helix: DNA overwinds when stretched. This small effect was previously observed using RBT, relying on long integration times⁴⁵. No subsequent studies have measured twist-stretch coupling in the freely fluctuating twist ensemble, although several groups have determined the sign and magnitude of the elastic coupling term by measuring changes in extension upon overwinding in the fixed twist ensemble⁴⁵⁻⁴⁷. Here, we have used AuRBT-80nm to perform rapid observations of twist-stretch coupling in a 4,130 bp DNA segment (**Fig. 3**). The DNA tether was torsionally constrained at the magnetic bead, but free to swivel at the coverslip, so that the rotor bead reported on the twist of the upper segment (**Fig. 3a**). Force was increased in ~1.5 pN steps from ~4.5 pN to ~13.5 pN, inducing stepwise helicity changes of ~0.01%. Helicity changes were well separated from Brownian noise using only 60 s of integration (**Fig. 3b,c**).

AuRBT reveals a transient DNA gyrase intermediate

As a representative system for AuRBT measurements of nucleoprotein complexes, we investigated the structural dynamics of DNA gyrase, an essential bacterial molecular motor that harnesses ATP hydrolysis to introduce supercoils into DNA⁵ (**Fig. 4**). Gyrase has been previously studied using RBT^{6,7}, and substeps in its mechanochemical cycle have been characterized by analyzing changes in angle and z at limiting [ATP]⁶. Single-molecule

gyrase traces are characterized by processive bursts of activity^{6,7}, in which each enzymatic cycle introduces two rotations due to duplex strand passage⁵. The dominant kinetic dwell in the cycle occurs in the Ω state, in which >100 bp of DNA contour length are sequestered but no supercoils are trapped in the complex⁶. An ATP-accelerated remodeling transition converts Ω into a chirally-wrapped intermediate dubbed the α state, which can be detected as a rotational substep at low [ATP]⁶. The chiral wrap is critical for guaranteeing that subsequent strand passage will directionally introduce supercoils, differentiating gyrase from other members of the type II topoisomerase family⁴⁸. Post-strand-passage states are presumed to be short-lived and were not detected in prior RBT experiments under any conditions⁶. At saturating [ATP], the α state was also undetectable, and even the dominant Ω dwell could not be visualized in every cycle^{6,7}. Spatiotemporal resolution has thus been a limiting factor in achieving a complete understanding of DNA gyrase mechanochemistry.

AuRBT-140nm/420bp (**Fig. 4a**) was used to study DNA gyrase at high resolution, yielding well-resolved Ω dwells even at saturating [ATP]. Rapid transient excursions to supercoil-trapping states (previously seen only at limiting [ATP]) are also visible in the angle traces (**Fig. 4b**), suggesting a more dynamic picture of gyrase mechanochemistry than was previously appreciated. Finally, simultaneous angle and z tracking (**Fig. 4b,c**) reveals a previously undetected intermediate: the otherwise contracted z signal often exhibits transient (~10-150 ms) excursions toward zero (marked with *); these excursions typically occur in between Ω dwells in successive cycles. To display the angle- z dynamics, **Figure 4b** uses a color scale to represent z . In an alternative depiction, **Figure 4c** plots a single trace on an angle- z plane, and uses a color scale to represent time. The excursions in z imply that the enzyme visits a structural state in which a substantial amount of DNA contour length is released from the enzyme. We have named this new state the ν state. In a speculative model (**Fig. 4e**) that incorporates the ν state and is consistent with our data (**Fig. 4b,c**), DNA is partially released after strand passage and must be recaptured in the Ω configuration to reset the enzyme for the next cycle. Partially released gyrase intermediates have been previously proposed based on static AFM images⁴⁹ or on indirect interpretations of tension-dependent enzyme behavior⁷, but never directly observed in a dynamic assay.

Probing ensembles with high-resolution torque spectroscopy

Over the past decade, a number of methods have been introduced for measuring the torque on a single DNA molecule^{18-23,25,28}. Among them, the optical torque wrench (OTW)^{28,50,51} uses a polarized optical trap to measure and apply torques. Magnetic torque tweezers (MTT)²² and electromagnetic torque tweezers (eMTT)²¹ use a vertical field for force application, with a small fixed (MTT) or controllable (eMTT) horizontal component to measure and apply biologically relevant torques. Soft magnetic tweezers¹⁸ differ in implementation, but also measure displacement in a weak magnetic potential, as do nanorod magnetic tweezers²⁵. Static RBT^{23,26} uses the deflection of a calibrated ‘transducer’ DNA segment to measure torque in the molecule. For any torque measurement technique that measures the displacement of a rotational probe with drag γ in a harmonic potential with stiffness κ , the RMS torque noise is given by an expression closely related to equation (1):

$$\sigma_{\tau} = \kappa \sqrt{\frac{2k_B T}{\kappa} \left(\frac{t_r}{t} - \left[\frac{t_r}{t} \right]^2 \left(1 - \exp\left(-\frac{t}{t_r}\right) \right) \right)} \quad (3)$$

where t is the integration time and t_r is the relaxation time, as before. In the limit of long integration times, this expression depends only on the rotational drag:

$$\sigma_{\tau} \approx \sqrt{\frac{2k_B T \gamma}{t}} \quad (4)$$

We reasoned that we could make precise DNA torque measurements on much shorter timescales than previously published methods, by adapting the “static RBT” method to use gold nanosphere probes (**Fig. 5**). We characterized the fluctuations of gold nanosphere rotors attached to DNA transducers, in order to confirm the expected gains in torque resolution (**Fig. 5b** and **Supplementary Fig. 6**). Up to 55X reductions in required integration times are seen relative to previous static RBT measurements, and even larger improvements are seen relative to other techniques.

To test the performance of static AuRBT on a well-characterized molecular system, we examined the B-Z transition in DNA molecules containing a 50 bp GC-repeat Sequence Of Interest (SOI)^{23,26}. This sequence (“Z50”) displays a localized transition from right-handed BDNA to left-handed Z-DNA under mild negative supercoiling⁵². As expected, we observed a characteristic torque signature that is well-described by a statistical mechanical model²³ similar to the Ising model at fixed magnetization (IMFM)⁵³. Upon unwinding, the B-DNA molecule initially builds up torque linearly. Further unwinding causes an abrupt torque jump corresponding to the formation of an initial Z-DNA domain. The domain can then be extended at approximately constant torque until the entire SOI is converted to Z-DNA, restoring linear elastic behavior.

AuRBT reveals the mean torque as a function of imposed twist at higher resolution than reported earlier, and validates the previously proposed model with high fidelity (**Fig. 5c**). Additionally, the improved sampling allows for a new kind of comparison between theory and experiment for this transition. Based on the best-fit parameters obtained from the averaged torque alone (black curve in **Fig. 5c**), we used the statistical mechanical model (**Supplementary Note 1**) to predict the entire distribution of measured torques at each value of total twist. This distribution can be compared with the experimental distribution obtained for each sampled twist value, and shows excellent agreement between theory and experiment. The comparison is shown in 2D histograms (**Fig. 5d-e**) and in an animated plot (**Supplementary Video 2**).

Discussion

Two major goals that drive the development of single-molecule approaches are (1) to directly observe dynamic transitions and fleeting intermediates in actively functioning biomolecular complexes (**Fig. 4**) and (2) to characterize distributions of molecular properties, as opposed to ensemble averages (**Fig. 5**). In practical single-molecule

manipulation experiments, slow Brownian fluctuations can interfere with both of these goals^{1,2}. For measurements of DNA twist and torque, AuRBT helps realize the potential of single-molecule analysis by providing the spatiotemporal resolution to detect intermediates, and the sampling power to define distributions. AuRBT allows biologically relevant angular displacements to be resolved on previously inaccessible timescales that are relevant to enzymology. For example, the twist signal expected from unwinding of a single DNA basepair can now be detected with less than 100 ms of integration; and larger changes can be resolved on ~1 ms timescales (**Fig. 2a**). When different measurement coordinates are available for detecting the same biomolecular event, direct angular measurements can now sometimes be the most sensitive alternative: for example, indirect measurements of ΔLk via plectonemic amplification¹⁰ require 1 s of integration or longer in order to discriminate single-bp differences in unwinding. Similarly, published high-resolution optical tweezers assays of DNA translocating motors require ~1 s of integration to discriminate changes in extension arising from single-bp steps^{1,16}. For the subset of DNA translocating motors that track the helical groove¹⁵, AuRBT may be used to detect single-bp steps on shorter timescales, by relying on the angular coordinate instead.

When comparing alternative methods for direct measurements of DNA twist and torque, AuRBT offers distinct advantages and some tradeoffs. AuRBT should be considered when high resolution is paramount: in comparison to some prominent alternatives, AuRBT enables precise twist measurements using >50,000× shorter integration times than FOMT¹³ (**Fig. 2a**) and precise torque measurements using >500× shorter integration times than OTW^{28,50,51} (**Fig. 5b**).

For twist measurements, FOMT has the compensatory advantage that it can be performed with minor modifications to many existing magnetic tweezers setups, and that a single molecule can easily be assayed successively in fixed-angle and freely-fluctuating modes¹³. Additionally, twist assays with larger probes — including FOMT and RBT³ — can generally be performed at lower forces than AuRBT, which relies on tension to suppress lateral fluctuations (**Supplementary Fig. 7**). The highest resolution AuRBT measurements reported here required a minimum of ~5 pN of tension, although high-resolution assays of the tension-sensitive DNA gyrase enzyme were performed (using 140 nm gold rotors) at ~1 pN. Similar tradeoffs between tension and resolution are seen in high-resolution optical trapping experiments, which require high tensions (typically >10 pN) to reduce tether compliance^{1,16}.

For torque measurements, OTW can be advantageous for some experiments because it also includes a simultaneous dynamic high-resolution force measurement. In addition, OTW (and MTT²² and related techniques) can be performed over a wide range of torques, whereas static AuRBT is restricted to the torque range over which the B-DNA transducer displays linear twist elasticity. This important limitation might be overcome in the future by using stable transducers constructed from DNA origami^{3,54,55}, expanding the accessible torque range.

AuRBT contributes to a new generation of single-molecule approaches in which high-resolution measurements of multiple degrees of freedom provide detailed dynamic pictures

of molecular processes. AuRBT combines direct measurements of angle with high-bandwidth extension measurements (**Supplementary Fig. 8**), which we exploited to discover a previously unknown structural intermediate in DNA gyrase (**Fig. 4**), opening the door for further dissections of gyrase mechanism and illustrating the potential for investigating other complex DNA:protein machines. Other recent high-resolution multiparameter methods have included an elegant combination of Ångstrom-resolution optical trapping with single-molecule fluorescence⁵⁶. In principle, there are no barriers to augmenting AuRBT with single-molecule fluorescence as well: AuRBT measurements are based entirely on near-infrared scattering, leaving the visible spectrum free for future experiments in which fluorescent probes report synchronously on internal degrees of freedom. Increasingly high-resolution and multidimensional single-molecule methods will help bridge the gap between atomically detailed crystal structures and dynamic functional assays, illuminating the complete conformational landscapes of molecular machines at the heart of biology.

METHODS

Instrumentation

Experiments were performed on a modified Nikon Eclipse Ti-S inverted microscope (**Supplementary Fig. 1**). Samples were mounted on a three-axis nanopositioning stage (Mad City Labs PDQ-series). Excitation was provided by an intensity-stabilized 845 nm laser diode (Lumics LU0845M200) directly coupled to a polarization-maintaining fiber; laser power fluctuations were $\pm 0.1\%$. Laser power used (measured after the fiber) ranged from 2.5 mW to 80 mW; the highest powers are required for the smallest beads. Under these conditions, nanoparticle heating and optical forces are generally small (**Supplementary Note 2**), and there was no evidence of optical damage, with many molecules lasting for hours of observation. The laser was collimated into a ~ 2 mm beam and then focused onto the objective back focal plane (see **Fig. 1** and **Supplementary Figs. 1,2**) using a 500 mm achromatic lens. A half-wave plate was used to achieve s-polarization at the sample interface. The return beam was collected on a position-sensitive detector (**Supplementary Fig. 1**) to provide a signal for focus stabilization⁵⁷, which was controlled by a Matlab callback function implementing proportional-integral gain at 1 Hz (**Supplementary Fig. 9**). Scattered light was collected with a Nikon Apo TIRF (60 \times / 1.49 oil) objective and imaged through an optical path splitter (Cairn, Optosplit II) and onto an EMCCD camera (Andor Ixon+) equipped with liquid cooling (Koolance Exos-2).

Magnetic tweezers were used to apply calibrated stretching forces. A pair of $\frac{1}{4} \times \frac{1}{4} \times \frac{1}{2}$ inch rectangular neodymium magnets (K&J Magnetics B448) was held above the sample in a machined aluminum mount with dipoles in opposing directions (**Fig. 1a**), as described previously^{6,58}. A hollowed shaft connected the magnets to a rotary servomotor (Physik Instrumente C-150.PD), which was mounted on a vertical servomotor (Physik Instrumente M-126.PD1) to enable rotation about and translation along the optical axis. Collimated light from a superbright LED (Thorlabs M660F1) entered the sample from above through a 0.6 mm gap in the magnets, providing illumination for 3D ring tracking of magnetic beads during force calibrations.

A complete list of parts for AuRBT is provided in **Supplementary Note 3**.

Preparation of DNA, beads, and protein

DNA tethers for rotor bead tracking were prepared by ligation of restriction enzyme digested PCR products (or hybridized oligonucleotides in the case of the Z50 SOI), as in previous work^{6,23,26}. The details of tether construction are shown in **Supplementary Table 3**. Magnetic beads were prepared by crosslinking 1 μm carboxy-modified superparamagnetic beads (MyOne, Invitrogen) with rabbit anti-fluorescein (Invitrogen)⁷. Rotor beads were neutravidin coated gold nanospheres (Nanopartz catalog numbers C11-70-TN-50, C11-90-TN-50, and C11-125-TN-50 for ~80 nm, ~110 nm, and ~140 nm beads respectively) or “Power-Bind*” streptavidin coated polystyrene spheres (Thermo Scientific; 300 nm beads). *E. coli* GyrA and GyrB subunits were individually expressed and purified as described⁵⁹, mixed to reconstitute tetramers, and stored at -80°C in 50 mM Tris-HCl, pH 7.5, 100 mM potassium glutamate, 2 mM DTT, 1 mM EDTA, and 10% glycerol.

Chamber preparation

Custom flow cells were made of laser-cut paraffin-based (Nescofilm) channels that were melted at 73°C between a 24×50 mm No. 1.5 glass coverslip (VWR) and a 24×50 mm hole-punched vinyl coverslip (Rinzle). Imaging was performed through the glass side, while watertight connections to polyethylene tubing (SAI, PE-10) were made at the ports on the vinyl side by using small rubber o-rings. Tubings were mated with o-rings after being pulled through undersized holes in custom machined aluminum bars, which also facilitated clamping of the o-rings to the surface. The bars compressed the o-rings against the vinyl coverslip ports, sealing the free end of the tubing in a small space near the channel entry port. The active surface of the glass coverslip was spin-coated with 0.1% w/v nitrocellulose (Ernest F. Fullam) in Amyl Acetate > 30 minutes prior to chamber assembly.

To prepare bead-DNA complexes, 25 μL of gold nanospheres were washed by centrifugation in 150 μL of binding buffer (500 mM NaCl, 40 mM Tris-HCl pH 8.0, 0.2% tween-20, 200 $\mu\text{g}/\text{mL}$ BSA, 5 mM EDTA and 0.01% sodium azide), resuspended in 25 μL of binding buffer, mixed with 3 μL of DNA tethers (~50 pM in 10 mM Tris-HCl pH 8.0 and 5 mM EDTA), and incubated overnight. Channel preparation began by flowing 40 μL of 2 $\mu\text{g}/\text{mL}$ anti-digoxigenin (Roche) in PBS and incubating for 60 minutes, and subsequently washing with 400 μL of passivation buffer (a one-to-one mixture of 10 mg/mL NEB BSA and a solution containing 1 M NaCl, 80 mM Tris-HCl pH 8.0, 0.4% tween-20, 10 mM EDTA and 0.02% sodium azide) and incubating for 1-2 hrs. After channel passivation, the bead-DNA mixture was introduced for 1hr, and then the channel was washed with 400 μL of binding buffer. Finally, 10 μL of magnetic beads in PBS were mixed with 15 μL of binding buffer and introduced for 1 hr, followed by an additional wash with 400 μL binding buffer. Twist-stretch coupling and torque spectroscopy measurements were performed in 40 mM Tris pH 8.0, 100mM NaCl, 5mM EDTA, 200 $\mu\text{g}/\text{mL}$ BSA (NEB), 0.01% sodium azide, and 0.2% tween-20. Gyrase experiments were performed in GB (35 mM Tris-HCl, pH 7.6, 24 mM potassium glutamate, 4 mM MgCl_2 , 2 mM DTT, 250 $\mu\text{g}/\text{mL}$ BSA (NEB), 0.2 mM spermidine, 0.2% tween-20 and 1 mM ATP), essentially as described previously⁶.

Selecting DNA tethers for AuRBT

To select a rotor bead assembly for analysis, the coverslip surface was first scanned to visually identify a scattering gold particle co-localized underneath a magnetic bead. A short bead tracking dataset was then acquired to check for expected rotor bead behavior. Beads were rejected from further analysis if the xy positions failed to form an annulus (**Fig. 1b**), if the beads showed periods of heavily restricted mobility (reflecting surface sticking), or if the angular signal was unconstrained (reflecting DNA nicking or unconstrained attachment). Magnets were then rotated to verify the attachment geometry. For bottom-constrained tethers (as in **Fig. 4a**), magnet rotation at low force did not cause the magnetic bead to approach the surface; for top-constrained tethers (as in **Fig. 3a**), the rotor bead angle followed the rotation of the magnets. For doubly-constrained tethers (as in **Fig. 5a**), we rejected molecules if rotation of the magnetic bead did not produce a corresponding rotation of the rotor bead attenuated by the expected partition ratio (the ratio of the lower segment length to that of the entire molecule).

Data acquisition and PSF fitting

Rotor bead images were recorded at frame rates of 1.9, 3.4, and 6.3 kHz for 140 nm, 110 nm, and 80 nm rotor beads, respectively. The EMCCD's 'isolated crop' mode at 10x10 pixels was used in all three cases to achieve the necessary frame rates. A quasi-real-time acquisition and analysis loop was run in Matlab at a loop rate of 1 Hz. During each loop, all available images were downloaded from the camera and immediately fit using a 2D Gaussian fitting function, which was written in C and compiled as a Matlab executable. Fit parameters included an additive offset c , peak height A , x -position x_o , y -position y_o , x -standard deviation σ_x , and y -standard deviation σ_y .

$$f=c+A \exp \left(-\frac{(x-x_o)^2}{2\sigma_x^2} - \frac{(y-y_o)^2}{2\sigma_y^2} \right)$$

After fitting, all raw images and fit parameters were written directly to a six-disk RAID array, and proportional feedback was applied to the sample stage to stabilize the x - y position of the molecule in the center of the crop.

Rotor bead tracking data analysis, calibration, and corrections

To calibrate x - y trajectories, lateral magnification was determined by scanning a surface-bound gold nanoparticle across a rectangular lattice of x - y positions, and tracking its position. Mean row and column separations gave an average magnification of 153x. Further corrections were applied to x - y trajectories before calculation of angle. First, residual drift was corrected by subtracting the center of an ellipse fitted to each one-second interval of data. Next, overall ellipticity was removed using a fit to the entire trajectory (see **Supplementary Fig. 10**). Rotor bead angle was determined by computing the four-quadrant inverse tangent of each corrected pair of (x,y) coordinates, and then unwrapping the result to determine cumulative angle (**Supplementary Video 1**). Bead sizes were determined by fitting histograms of measured radii to Rician distributions⁶⁰, in order to extract each orbital radius independent of lateral fluctuations.

Rotor bead heights were determined using evanescent nanometry^{29,30}, computed as $\Delta z = -\lambda \log(I/I_\phi)$ where I is proportional to the instantaneous scattering intensity, and determined by 2D Gaussian fitting ($I \equiv A\sigma_x\sigma_y$) and $\langle I \rangle_\phi$ represents the average scattering intensity at a given in-plane angle ϕ (see **Supplementary Figure 11**). The field's decay length λ was determined by cross-calibration with dual focus imaging (see **Supplementary Fig. 3**). Evanescent field decay lengths were typically 130-200 nm.

To allow unambiguous angle tracking, lateral fluctuations of the rotor bead were suppressed by tension. Rare zero crossings (in which a bead trajectory passes through the x-y origin, causing erroneous jumps of integer rotations) were identified and corrected for using semi-automated analysis in Matlab. Tensions were chosen to give a maximum tolerated zero crossing rate of ~10-20 per million frames; these conditions also ensure that positional noise contributes negligible errors to angle determination (**Supplementary Fig. 7**).

Force calibration

The average force as a function of magnet height was computed as the product of lateral stiffness along the field direction with the extension of the molecule⁶¹. Lateral stiffness was estimated from Lorentzian fits to position noise power spectra⁶² generated from 70,000 image frames taken at a sampling rate of 1.6 kHz (the maximum observed Lorentzian cutoff frequency of ~ 50 Hz). At each magnet position, the focal depth of the magnetic bead was determined relative to the feedback-stabilized focal plane by using a lookup table for the radial profile of its diffraction ring pattern as a function of defocus⁶³. Absolute DNA extension was determined by comparing the focal depth of the tethered bead to that of a surface-bound reference bead, and correcting for off-center attachments⁶⁴.

Torque spectroscopy

Static AuRBT torque spectroscopy was performed under 5 pN of tension. Torque-twist curves were acquired by rotating the magnetic tweezers at 18°/s from +5 rotations to -15 rotations and back. The magnet angle corresponding to $\theta = 0$ was determined by finding the magnet position which maximized extension of the molecule, as in references^{23,26}. The torsional rigidity of the transducer segment was determined by analyzing the noise power spectra of free twist fluctuations in top constrained molecules, which contained the identical DNA transducer.

Supplementary Material

Refer to Web version on PubMed Central for supplementary material.

ACKNOWLEDGEMENTS

We would like to thank J.M. Berger and members of the Bryant group for many useful discussions and comments on the manuscript; and A. Bekshaev, P. Ruijgrok, and M. Dijk for providing Matlab code used for computing Mie scattering parameters and optical forces. This work was supported by a Stanford Interdisciplinary Graduate Fellowship (SIGF) and the Natural Sciences and Engineering Research Council of Canada (award NSERC PGS-D3) to P.L.; by a Stanford Bio-X graduate fellowship to A.B.; by a Pew Scholars Award and NIH Grants No. OD004690 and GM106159 to Z.B.; and by a Swiss National Science Foundation Fellowship to F.C.O.

REFERENCES

1. Moffitt JR, Chemla YR, Smith SB, Bustamante C. Recent advances in optical tweezers. *Annual Review of Biochemistry*. 2008; 77:205–28.
2. Neuman KC, Nagy A. Single-molecule force spectroscopy: optical tweezers, magnetic tweezers and atomic force microscopy. *Nat Methods*. 2008; 5:491–505. [PubMed: 18511917]
3. Bryant Z, Oberstrass FC, Basu A. Recent developments in single-molecule DNA mechanics. *Current Opinion in Structural Biology*. 2012; 22:304–312. [PubMed: 22658779]
4. Vologodskii A. Determining protein-induced DNA bending in force-extension experiments: theoretical analysis. *Biophys J*. 2009; 96:3591–9. [PubMed: 19413964]
5. Nollmann M, Crisona NJ, Arimondo PB. Thirty years of Escherichia coli DNA gyrase: from in vivo function to single-molecule mechanism. *Biochimie*. 2007; 89:490–9. [PubMed: 17397985]
6. Basu A, Schoeffler AJ, Berger JM, Bryant Z. ATP binding controls distinct structural transitions of Escherichia coli DNA gyrase in complex with DNA. *Nat Struct Mol Biol*. 2012; 19:538–46. S1. [PubMed: 22484318]
7. Gore J, et al. Mechanochemical analysis of DNA gyrase using rotor bead tracking. *Nature*. 2006; 439:100–4. [PubMed: 16397501]
8. Killian JL, Li M, Sheinin MY, Wang MD. Recent advances in single molecule studies of nucleosomes. *Current Opinion in Structural Biology*. 2012; 22:80–7. [PubMed: 22172540]
9. Kornberg RD, Lorch Y. Twenty-five years of the nucleosome, fundamental particle of the eukaryote chromosome. *Cell*. 1999; 98:285–94. [PubMed: 10458604]
10. Revyakin A, Liu C, Ebright RH, Strick TR. Abortive initiation and productive initiation by RNA polymerase involve DNA scrunching. *Science*. 2006; 314:1139–43. [PubMed: 17110577]
11. Lee M, Lipfert J, Sanchez H, Wyman C, Dekker NH. Structural and torsional properties of the RAD51-dsDNA nucleoprotein filament. *Nucleic Acids Research*. 2013; 41:7023–7030. [PubMed: 23703213]
12. Arata H, et al. Direct observation of twisting steps during Rad51 polymerization on DNA. *Proceedings of the National Academy of Sciences of the United States of America*. 2009; 106:19239–44. [PubMed: 19884492]
13. Lipfert J, Wiggin M, Kerssemakers JW, Pedaci F, Dekker NH. Freely orbiting magnetic tweezers to directly monitor changes in the twist of nucleic acids. *Nature Communications*. 2011; 2:439.
14. Corbett KD, Berger JM. Structure, molecular mechanisms, and evolutionary relationships in DNA topoisomerases. *Annu Rev Biophys Biomol Struct*. 2004; 33:95–118. [PubMed: 15139806]
15. Harada Y, et al. Direct observation of DNA rotation during transcription by Escherichia coli RNA polymerase. *Nature*. 2001; 409:113–5. [PubMed: 11343125]
16. Abbondanzieri EA, Greenleaf WJ, Shaevitz JW, Landick R, Block SM. Direct observation of base-pair stepping by RNA polymerase. *Nature*. 2005; 438:460–5. [PubMed: 16284617]
17. Li G, Levitus M, Bustamante C, Widom J. Rapid spontaneous accessibility of nucleosomal DNA. *Nature structural & molecular biology*. 2005; 12:46–53.
18. Mosconi F, Allemand JF, Croquette V. Soft magnetic tweezers: a proof of principle. *Rev Sci Instrum*. 2011; 82:034302. [PubMed: 21456769]
19. Forth S, Sheinin MY, Inman J, Wang MD. Torque measurement at the single-molecule level. *Annual Review of Biophysics*. 2013; 42:583–604.
20. Bryant Z, et al. Structural transitions and elasticity from torque measurements on DNA. *Nature*. 2003; 424:338–41. [PubMed: 12867987]
21. Janssen XJ, et al. Electromagnetic torque tweezers: a versatile approach for measurement of single-molecule twist and torque. *Nano Lett*. 2012; 12:3634–9. [PubMed: 22642488]
22. Lipfert J, Kerssemakers JW, Jager T, Dekker NH. Magnetic torque tweezers: measuring torsional stiffness in DNA and RecA-DNA filaments. *Nat Methods*. 2010; 7:977–980. [PubMed: 20953173]
23. Oberstrass FC, Fernandes LE, Bryant Z. Torque measurements reveal sequence-specific cooperative transitions in supercoiled DNA. *Proceedings of the National Academy of Sciences of the United States of America*. 2012; 109:6106–6111. [PubMed: 22474350]

24. Forth S, et al. Abrupt buckling transition observed during the plectoneme formation of individual DNA molecules. *Physical Review Letters*. 2008; 100:148301. [PubMed: 18518075]
25. Celedon A, et al. Magnetic tweezers measurement of single molecule torque. *Nano Lett*. 2009; 9:1720–5. [PubMed: 19301859]
26. Oberstrass FC, Fernandes LE, Lebel P, Bryant Z. Torque Spectroscopy of DNA: Base-Pair Stability, Boundary Effects, Backbending, and Breathing Dynamics. *Physical Review Letters*. 2013; 110:178103. [PubMed: 23679785]
27. Patel SS, Donmez I. Mechanisms of helicases. *J Biol Chem*. 2006; 281:18265–8. [PubMed: 16670085]
28. Deufel C, Forth S, Simmons CR, Dejgosh S, Wang MD. Nanofabricated quartz cylinders for angular trapping: DNA supercoiling torque detection. *Nat Methods*. 2007; 4:223–5. [PubMed: 17322891]
29. Zocchi G. Proteins unfold in steps. *Proceedings of the National Academy of Sciences of the United States of America*. 1997; 94:10647–51. [PubMed: 9380689]
30. Liu R, Garcia-Manyes S, Sarkar A, Badilla CL, Fernandez JM. Mechanical characterization of protein L in the low-force regime by electromagnetic tweezers/evanescent nanometry. *Biophys J*. 2009; 96:3810–21. [PubMed: 19413987]
31. Yasuda R, Noji H, Yoshida M, Kinosita K Jr, Itoh H. Resolution of distinct rotational substeps by submillisecond kinetic analysis of F1-ATPase. *Nature*. 2001; 410:898–904. [PubMed: 11309608]
32. Dunn AR, Spudich JA. Dynamics of the unbound head during myosin V processive translocation. *Nat Struct Mol Biol*. 2007; 14:246–8. [PubMed: 17293871]
33. Lindner M, et al. Force-free measurements of the conformations of DNA molecules tethered to a wall. *Phys Rev E Stat Nonlin Soft Matter Phys*. 2011; 83:011916. [PubMed: 21405722]
34. Braslavsky I, et al. Objective-type dark-field illumination for scattering from microbeads. *Applied Optics*. 2001; 40:5650–7. [PubMed: 18364854]
35. Dunn AR, Chuan P, Bryant Z, Spudich JA. Contribution of the myosin VI tail domain to processive stepping and intramolecular tension sensing. *Proceedings of the National Academy of Sciences of the United States of America*. 2010; 107:7746–50. [PubMed: 20385849]
36. Ueno H, et al. Simple dark-field microscopy with nanometer spatial precision and microsecond temporal resolution. *Biophys J*. 2010; 98:2014–23. [PubMed: 20441766]
37. Mashanov GI, Tacon D, Knight AE, Peckham M, Molloy JE. Visualizing single molecules inside living cells using total internal reflection fluorescence microscopy. *Methods*. 2003; 29:142–52. [PubMed: 12606220]
38. Friedman LJ, Chung J, Gelles J. Viewing dynamic assembly of molecular complexes by multi-wavelength single-molecule fluorescence. *Biophys J*. 2006; 91:1023–31. [PubMed: 16698779]
39. Wong WP, Halvorsen K. The effect of integration time on fluctuation measurements: calibrating an optical trap in the presence of motion blur. *Opt Express*. 2006; 14:12517–31. [PubMed: 19529687]
40. Yasuda R, Miyata H, Kinosita K Jr. Direct measurement of the torsional rigidity of single actin filaments. *Journal of Molecular Biology*. 1996; 263:227–36. [PubMed: 8913303]
41. Arunajadai SG, Cheng W. Step detection in single-molecule real time trajectories embedded in correlated noise. *PLoS One*. 2013; 8:e59279. [PubMed: 23533612]
42. Aggarwal T, Materassi D, Davison R, Hays T, Salapaka M. Detection of Steps in Single Molecule Data. *Cell Mol Bioeng*. 2012; 5:14–31. [PubMed: 23956798]
43. Wallin AE, Salmi A, Tuma R. Step length measurement--theory and simulation for tethered bead constant-force single molecule assay. *Biophys J*. 2007; 93:795–805. [PubMed: 17496045]
44. Milescu LS, Yildiz A, Selvin PR, Sachs F. Extracting dwell time sequences from processive molecular motor data. *Biophys J*. 2006; 91:3135–50. [PubMed: 16905607]
45. Gore J, et al. DNA overwinds when stretched. *Nature*. 2006; 442:836–9. [PubMed: 16862122]
46. Lionnet T, Joubaud S, Lavery R, Bensimon D, Croquette V. Wringing out DNA. *Physical Review Letters*. 2006; 96:178102. [PubMed: 16712339]
47. Sheinin MY, Wang MD. Twist-stretch coupling and phase transition during DNA supercoiling. *Physical Chemistry Chemical Physics*. 2009; 11:4800–3. [PubMed: 19506753]

48. Schoeffler AJ, Berger JM. DNA topoisomerases: harnessing and constraining energy to govern chromosome topology. *Quarterly Reviews of Biophysics*. 2008; 41:41–101. [PubMed: 18755053]
49. Heddle JG, Mittelheiser S, Maxwell A, Thomson NH. Nucleotide binding to DNA gyrase causes loss of DNA wrap. *J Mol Biol*. 2004; 337:597–610. [PubMed: 15019780]
50. Gutierrez-Medina B, Andreasson JO, Greenleaf WJ, Laporta A, Block SM. An optical apparatus for rotation and trapping. *Methods in Enzymology*. 2010; 475:377–404. [PubMed: 20627165]
51. La Porta A, Wang MD. Optical torque wrench: angular trapping, rotation, and torque detection of quartz microparticles. *Physical Review Letters*. 2004; 92:190801. [PubMed: 15169392]
52. Nordheim A, et al. Negatively supercoiled plasmids contain left-handed Z-DNA segments as detected by specific antibody binding. *Cell*. 1982; 31:309–18. [PubMed: 7159926]
53. Gulminelli F, et al. Transient backbending behavior in the Ising model with fixed magnetization. *Phys Rev E Stat Nonlin Soft Matter Phys*. 2003; 68:026119. [PubMed: 14525061]
54. Kauert DJ, Kurth T, Liedl T, Seidel R. Direct mechanical measurements reveal the material properties of three-dimensional DNA origami. *Nano Lett*. 2011; 11:5558–63. [PubMed: 22047401]
55. Pfitzner E, et al. Rigid DNA Beams for High-Resolution Single-Molecule Mechanics. *Angew Chem Int Ed Engl*. 2013; 52:7766–7771. [PubMed: 23794413]
56. Comstock MJ, Ha T, Chemla YR. Ultrahigh-resolution optical trap with single-fluorophore sensitivity. *Nat Methods*. 2011; 8:335–40. [PubMed: 21336286]
57. Huang B, Jones SA, Brandenburg B, Zhuang X. Whole-cell 3D STORM reveals interactions between cellular structures with nanometer-scale resolution. *Nat Methods*. 2008; 5:1047–52. [PubMed: 19029906]
58. Lipfert J, Hao X, Dekker NH. Quantitative modeling and optimization of magnetic tweezers. *Biophys J*. 2009; 96:5040–9. [PubMed: 19527664]
59. Tretter EM, Berger JM. Mechanisms for defining supercoiling set point of DNA gyrase orthologs: I. A nonconserved acidic C-terminal tail modulates *Escherichia coli* gyrase activity. *J Biol Chem*. 2012; 287:18636–44. [PubMed: 22457353]
60. Rice S. Mathematical analysis of random noise. *Bell system technical journal*. 1945; 24:46–156.
61. Strick TR, Allemand JF, Bensimon D, Bensimon A, Croquette V. The elasticity of a single supercoiled DNA molecule. *Science*. 1996; 271:1835–7. [PubMed: 8596951]
62. te Velthuis AJ, Kerssemakers JW, Lipfert J, Dekker NH. Quantitative guidelines for force calibration through spectral analysis of magnetic tweezers data. *Biophys J*. 2010; 99:1292–302. [PubMed: 20713015]
63. Gosse C, Croquette V. Magnetic tweezers: micromanipulation and force measurement at the molecular level. *Biophys J*. 2002; 82:3314–29. [PubMed: 12023254]
64. Klaue D, Seidel R. Torsional stiffness of single superparamagnetic microspheres in an external magnetic field. *Physical Review Letters*. 2009; 102:028302. [PubMed: 19257322]

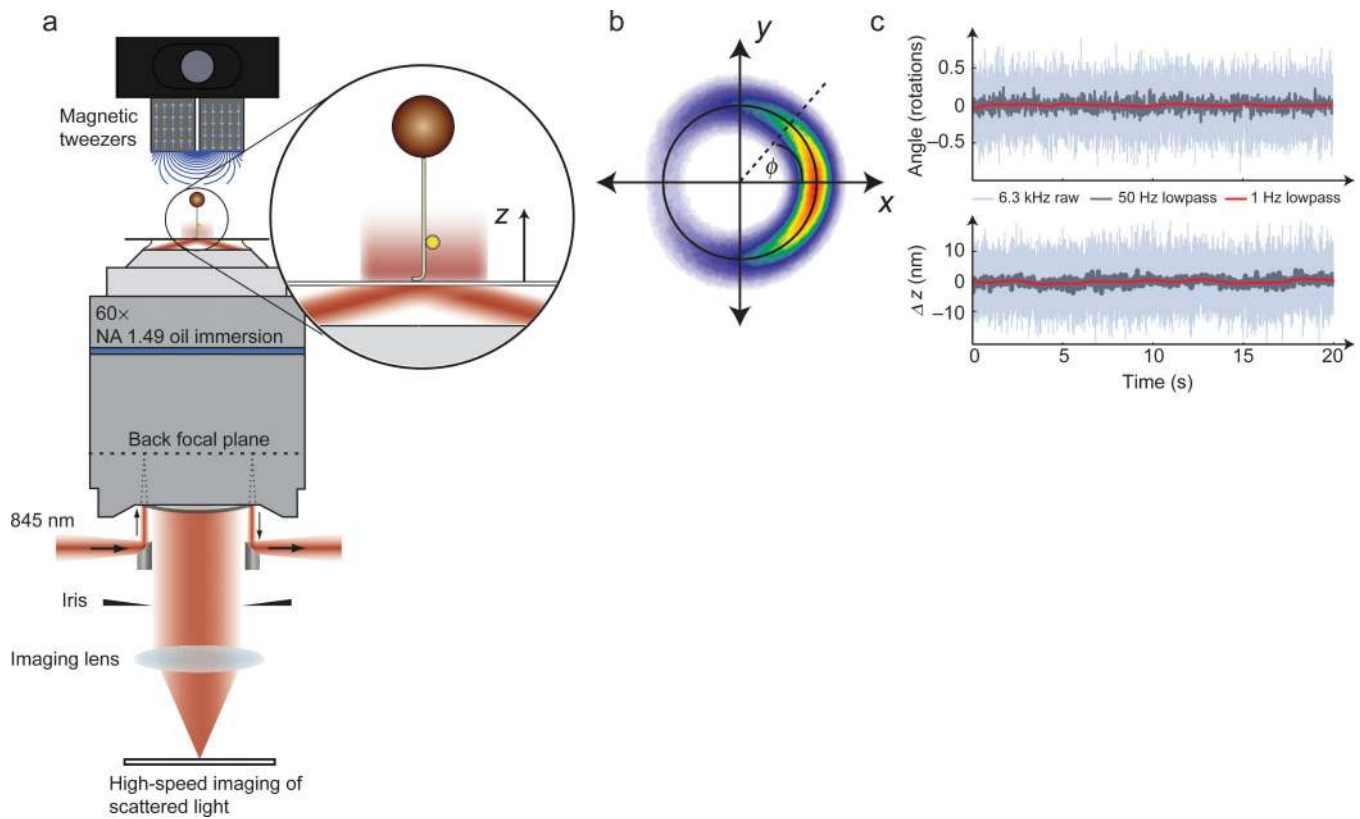


Figure 1. AuRBT design and data collection

(a) Combining 3D nanoparticle tracking with magnetic tweezers. An excitation laser is introduced using a small 45-degree mirror to achieve total internal reflection. The return beam is extracted using a second mirror, and stray light is rejected with an iris. The darkfield image of a gold rotor bead is imaged on a high-speed camera. Evanescent illumination excludes the larger magnetic bead from the excitation field, while providing an intensity gradient for tracking z displacements. (b) 2D tracking (see also **Supplementary Video 1**). A rotor bead was attached above a 420 bp torsionally constrained DNA segment and held under 10 pN of tension. The XY position was recorded at 6.3 kHz and accumulated over 150 s to generate a 2D histogram, which shows restriction to an annulus and a preferred equilibrium angle. The instantaneous in-plane angle ϕ can be calculated from the x and y measurements. The measured diameter of the orbit for this bead (black circle) is $d = 69.4$ nm, which is a measure of the size of the particle. (c) Simultaneous angle and extension measurements of a rotor ($d = 68.1$ nm) attached above a 420 bp torsionally constrained segment and held under 26 pN of tension by a magnetic bead dimer. Extension was measured using evanescent nanometry (see **Methods** and **Supplementary Fig. 3**). Full-bandwidth traces are shown along with 50 Hz and 1 Hz lowpass filtered data.

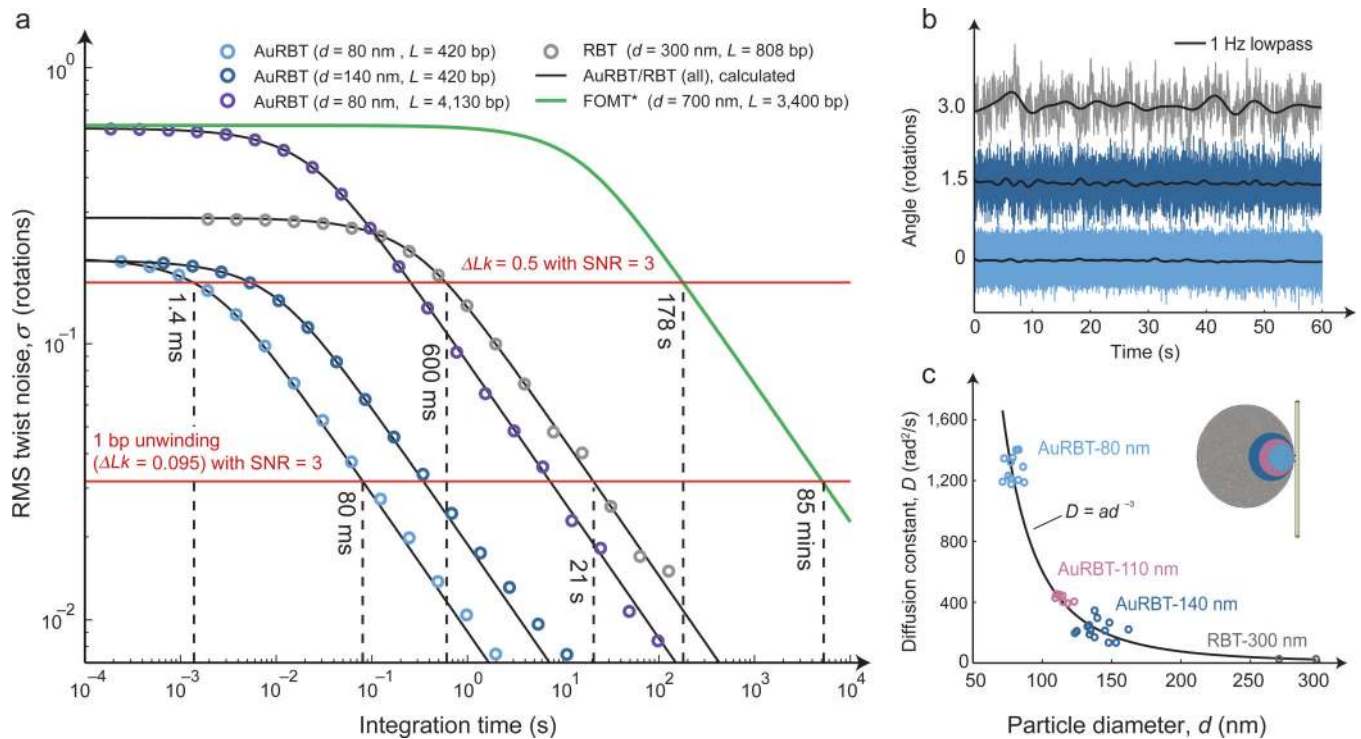


Figure 2. Angular resolution of AuRBT

(a) Reduction of Brownian twist noise as a function of integration time. Data points for the indicated probe sizes and tether lengths were obtained by computing the angular standard deviation across time-averaged data bins of varying sizes. Model curves were computed from Equation 1 using the torsional stiffness κ and relaxation time τ , obtained from separate fits to noise power spectral density plots (**Supplementary Fig. 4** and **Supplementary Table 1**). Dashed lines illustrate the integration times required to achieve an SNR value of 3 for the indicated signal sizes (SNR = 3 is chosen as an example; different SNR values may be desired, depending on the application). Plots were generated using raw data traces sampled for 63 s (AuRBT-80nm/420bp), 350 s (AuRBT-140nm/420bp), 785 s (AuRBT-80nm/4130bp), and 505 s (RBT-300nm/808bp). *The theoretical FOMT curve is calculated from the most favorable parameters reported in reference 13. (b) Full-bandwidth (color) and lowpass filtered (black) angle traces for various probe and tether combinations. Light blue: 80 nm probe / 420 bp tether, dark blue: 140 nm / 420 bp, gray: 300 nm / 808 bp. (c) Cubic scaling of rotational drag. For 36 different rotor beads, rotational diffusion constants D were measured by analyzing noise power spectra (as in **Supplementary Fig. 4**) and orbital diameters d were fit to the annulus of 2D positions (as in **Fig. 1b**). A plot of D vs d was fit to a cubic function: $D = ad^3$; small deviations from this model are expected to occur due to surface proximity (**Supplementary Fig. 5**).

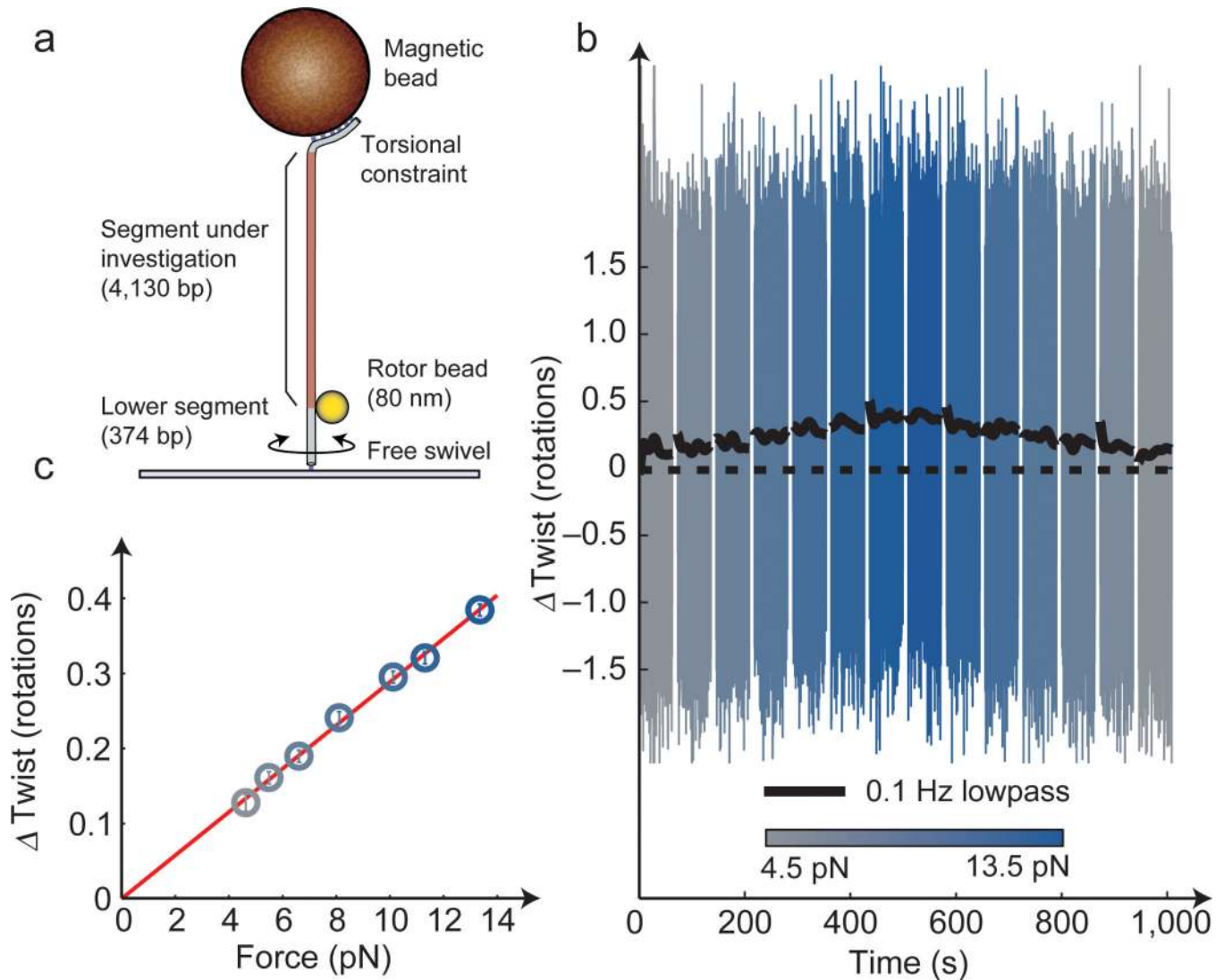


Figure 3. High-resolution measurement of twist-stretch coupling

(a) “Top-constrained” experimental geometry for measuring changes of twist in a long DNA segment. As in dynamic RBT^{3,23}, the rotor angle reflects the twist in the upper DNA segment. 80 nm rotors were used in order to maximize resolution. (b) Full-bandwidth (color) and filtered (black) angle traces for a DNA molecule, acquired during stepwise increments of tension exerted every 60 s. Each step of ~ 1.5 pN caused a change in DNA helicity change of $\sim 0.01\%$, and was detected with a SNR of ~ 4 . This experiment may be compared with figure 1c of reference 45, in which $\sim 10\times$ longer integration times were used to resolve changes in twist induced by $\sim 3\times$ larger steps in force. (c) Mean twist as a function of force, taken from the data shown in (b), showing the linear increase expected for a negative twist-stretch coupling coefficient⁴⁵. Error bars show the estimated RMS twist noise (see Fig. 2b) for the integration time $t = 120$ s (totaled over two 60 s dwells at each force). Similar results were obtained for a total of twelve individual DNA tethers.

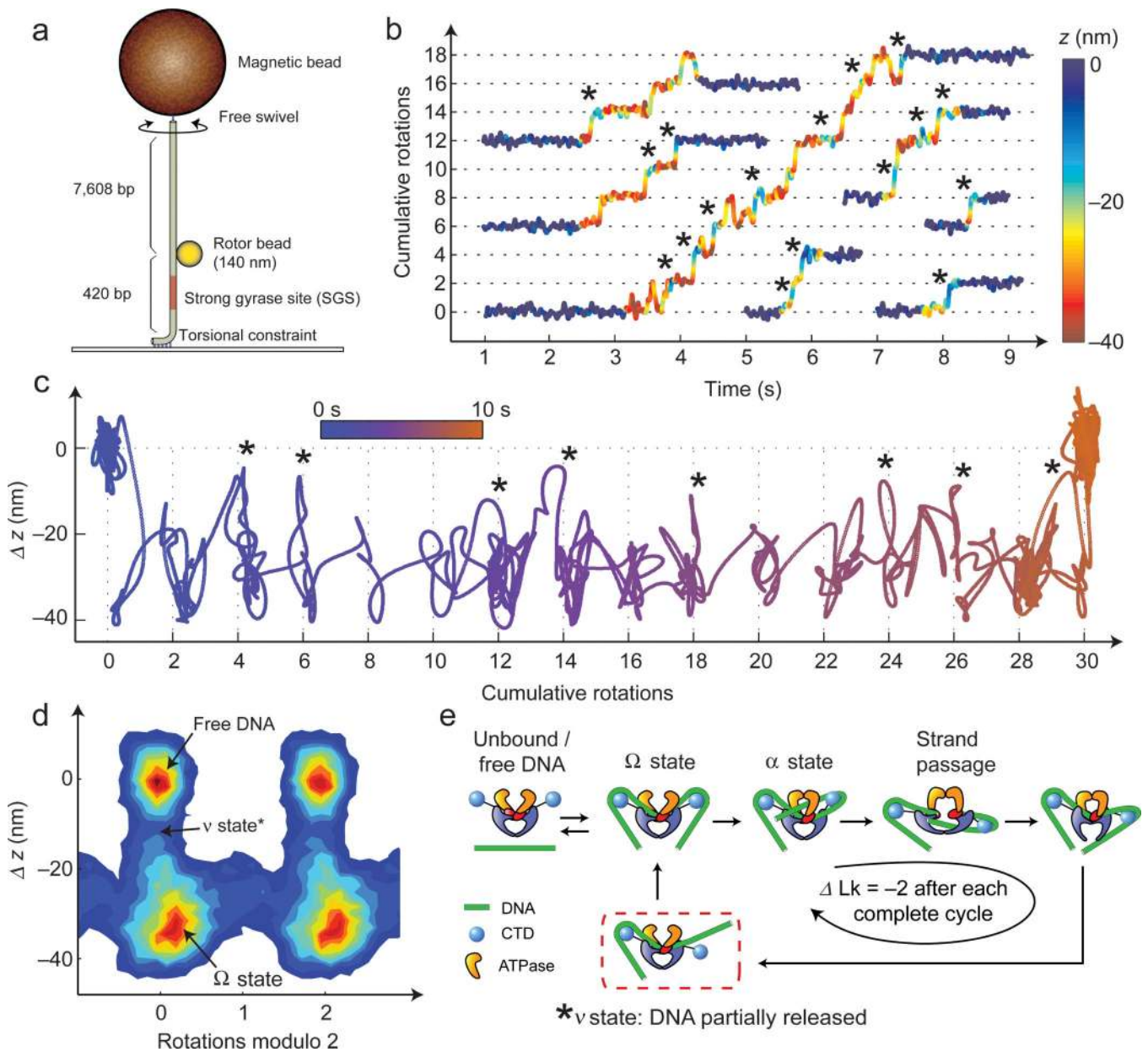


Figure 4. High-resolution analysis of gyrase dynamics at 1 mM [ATP]

(a) “Bottom-constrained” experimental geometry. During gyrase activity, the angle and height of the bead reflect changes in Lk and extension of the lower DNA segment^{3,6}. Measurements were performed using 140 nm rotors under 1.1 pN of tension, and angle and z were both lowpass filtered to 50 Hz. (b) Excised traces of single-enzyme bursts. Angle is plotted as a function of time, with color (blue to red) indicating the instantaneous value of DNA extension. Dominant dwells are visible every two rotations as expected⁶. Short regions flanking each burst show the extension of free DNA. Asterisks mark events in which the DNA extension briefly increases, primarily coinciding with entrance into a new rotational dwell. (c) A single gyrase trace is shown projected along angle and z -axes; brief excursions (*) are visible between dominant dwells. Color represents time, progressing from blue to

orange. **(d)** 2D histogram of angle and z coordinates⁶ accumulated over a total of 97 gyrase cycles belonging to 19 enzymatic bursts on five separate DNA tethers; 1.5 s of data flanking each burst were included to show the position of free DNA. **(e)** Proposed model explaining excursions in extension (*). DNA contour length is released from one or both CTDs after strand passage, entering a newly defined ν state. The DNA is then recaptured to reset the enzyme for the next cycle.

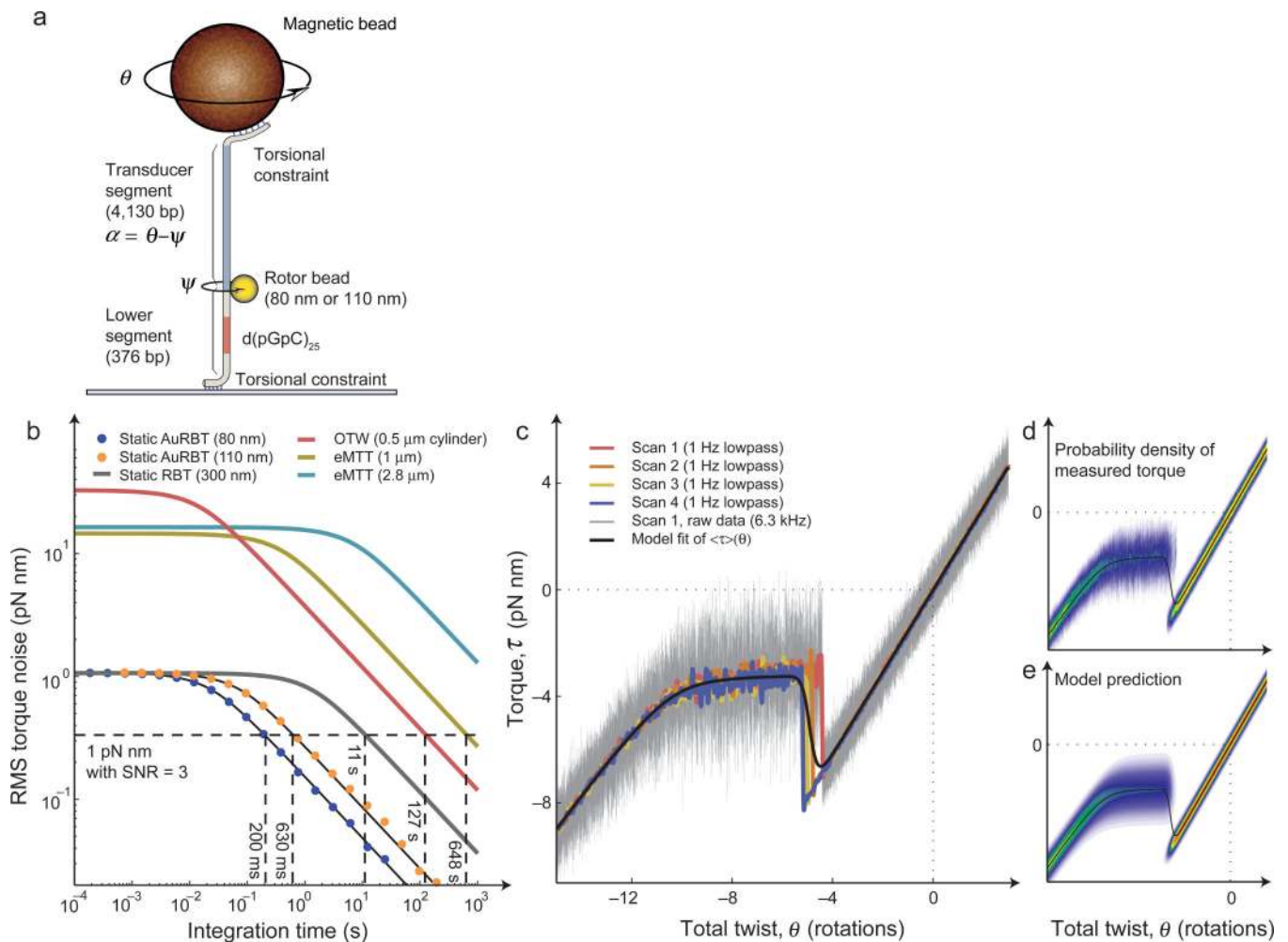


Figure 5. AuRBT torque spectroscopy

(a) “Doubly-constrained” experimental geometry for static torque measurements^{3,23,26}.

Total twist θ can be varied by rotating the magnets, and torque is measured from the angular deflection of a calibrated transducer segment, $\tau = \kappa\alpha$. A sequence of interest (SOI) can be placed in the lower segment, such as the 50 bp GC repeat used here to examine Z-DNA formation. (b) Torque resolution of AuRBT and of published alternative methods for measuring DNA torque. RMS torque noise was measured as a function of integration time, using 4130 bp transducer segments assayed in a “top-constrained” geometry. (The 80 nm rotor results are plotted from the same dataset as AuRBT-80nm/4,130bp in **Figure 2a**.)

Corresponding power spectral density plots are shown in **Supplementary Figure 6**. Models (Equation 3) were parameterized from spectral analysis for AuRBT and RBT and based on reported parameters for eMTT²¹, and OTW⁵⁰. The dashed horizontal line indicates the RMS torque noise required for measuring a 1 pN nm change with a signal-to-noise ratio of three, and its intersection point with each curve indicates the necessary duration of signal averaging. (c) Torque as a function of imposed twist for a DNA molecule containing a 50 bp GC-repeat. (Similar traces were obtained for a total of four molecules under two buffer conditions.) AuRBT-110 was used under 5 pN of tension, and twist was ramped linearly at 0.05 rotations/s. Lowpass filtered data for four individual rewinding curves on the same

molecule are shown as colored traces, and full-bandwidth data (6.3 kHz) are shown in gray. A statistical mechanical model for the B-Z transition^{23,26} was used to fit $\langle \tau \rangle(\theta)$ to the collection of four curves ($J = 4.55$ kcal/mol, $\Delta G = 0.47$ kcal/(mol bp), $1/\kappa_0 = 4.07$ rad/(pN nm), $\Delta c_t = 0.015$ rad/(pN nm bp), and $\Delta\theta = -1.03$ rad/bp). **(d-e)** Distributions of measured torque as a function of imposed twist (see also **Supplementary Video 2**). The expectation torque curve from (c) is replotted in black. **(d)** The combined full-bandwidth data from all traces in (c) were binned in order to plot $P(\tau)$ (heat-mapped) for each value of twist. **(e)** The predicted $P(\tau)$ was calculated (equations S9-S12) based on the parameters determined from fitting the expectation torque curve, and plotted for comparison with experiment.